ON THE INSTABILITY OF A SPRING-MOUNTED CIRCULAR CYLINDER IN A VISCOUS FLOW AT LOW REYNOLDS NUMBERS

C. Cossu

Laboratoire d'Hydrodynamique (LadHyX), CNRS-UMR 7646
École Polytechnique, F-91128 Palaiseau Cedex, France

AND

L. Morino

Dipartimento di Ingegneria Meccanica e Industriale, Università di Roma Tre
Via della Vasca Navale 79, I-00146 Roma, Italy

The first instability of a spring-mounted, damped, rigid circular cylinder, immersed in a viscous flow and free to move in a direction orthogonal to the unperturbed flow, is investigated by a global stability analysis. The flow is modelled by the full Navier–Stokes equations. For low ratios of the fluid density to the structure density, the von Karman mode is always the critical one and the critical Reynolds number, about 47, is nearly the same as for a stationary cylinder. In this case, for low structural damping, two complex modes are active and chaos is possible near the bifurcation. For higher density ratios, the critical Reynolds number decreases to less than the half the critical Reynolds number for a stationary structure. In this case, only a complex mode is active and chaotic behaviour does not seem to be possible near the bifurcation threshold.   © 2000 Academic Press

1. INTRODUCTION

IN 1985, SREENIVASAN OBSERVED different chaotic transition scenarios in the circular-cylinder wake at low Reynolds numbers. These observations led to a number of studies to find out if a low-dimensional chaotic attractor could explain the turbulent dynamics in open flows such as wakes, mixing layers and boundary layers. Van Atta & Gharib (1987) recognized that aeroelastic effects could also play a role in producing chaotic behaviour. Since then, the fluid-dynamics community has concentrated on the problem of the wake of a *stationary* circular cylinder and on its dynamics; Williamson (1996) gives a review on recent advances in this field. For this problem, it is now well established that the first instability is a Hopf bifurcation (Mathis *et al.* 1984; Sreenivasan *et al.* 1987; Jackson 1987) which occurs at a Reynolds number of about 47 and a Strouhal number slightly less than 0.12. At the onset of this global instability, a finite region of the near wake is absolutely unstable (Monkewitz 1988; Huerre & Monkewitz 1990). Olinger (1990) attributed the early observation of Sreenivasan to three-dimensional effects, while Abarbanel *et al.* (1991) suggested that finite size effects of the wind tunnel may also have been relevant. Considering moving cylinders, Olinger & Sreenivasan (1988) studied the nonlinear dynamics in the wake of an oscillating cylinder at low Reynolds numbers in the case of externally imposed oscillations. They observed a period doubling cascade leading to chaos and deduced a strong analogy with the

sine circle map dynamics. Concerning the study of vortex-induced vibrations of bluff bodies, the aeroelastic community has been interested mainly in the high Reynolds-number regime, where one usually has to resort to some empirical modelling of the fluid–structure interaction [see, for instance, Blevins (1991)].

In this study the first instability of the aeroelastic system composed of a rigid circular cylinder immersed in a viscous flow is investigated numerically by a global (in the sense defined by Huerre & Monkewitz 1990) stability analysis. The cylinder is spring-mounted, damped, and free to move in the direction perpendicular to the undisturbed flow. The fluid is modelled by the full two-dimensional Navier–Stokes equations without resorting to any empirical modelling. The main objective of the present analysis is to study the spectrum and the linear modes of the *coupled* system near the global instability threshold. The linear analysis will provide a description of the "active" modes that interact nonlinearly near the bifurcation, and is therefore a necessary step before going to the nonlinear analysis of vortex-induced vibrations at low Reynolds number which may explain the observations of Van Atta and Gharib (1987).

An integro-differential vorticity-only formulation, that uses Wu's integral representation of the velocity field (Wu & Thomson 1973) and integral constraints on the vorticity field (Wu 1976), is used to represent the Navier–Stokes equations. This approach allows one to limit the numerical-solution domain to the vortical region of the flow. The formulation, coupled with the structural motion equations, is then discretized to obtain a finite-dimensional system of ordinary differential equations with quadratic nonlinearities. The state vector of this discretized system is composed of the vorticity values at the grid nodes in the fluid domain, a global circulation variable, and the cylinder position and velocity. The parameters of the system are the Reynolds number based on the cylinder diameter $\mathrm{Re} = DU_\infty/\nu$, the fluid/solid density ratio $n = \rho_f/\rho_c$, the structural natural circular frequency ω_c, and the structural damping γ. We consider the Reynolds number Re as a "purely fluid" parameter because it is the only parameter governing the system when the structure is stationary. The structural natural circular frequency ω_c and damping γ are the "purely structural" parameters as they rule the system in the absence of fluid. The fluid/solid density ratio n is the coupling parameter. For every set of parameters considered, the equilibrium solution is found and then its stability is determined by numerically evaluating the spectrum of the linearized operator. The algorithm has been validated for the stationary circular cylinder (Cossu 1997; Cossu & Morino 1997).

For low density ratios n, two significant modes are identified: the "nearly-structural" mode, and the von Karman mode. The nearly-structural mode corresponds to eigenvalues that, in the limit $n \to 0$, tend to the characteristic (complex) frequency of the structure in the absence of fluid. The von Karman mode corresponds to eigenvalues almost identical to the critical eigenvalues of the "purely fluid" system with a stationary structure. The two modes are described for different structural natural frequencies; the influence of the density ratio on their stability is also analysed.

The mathematical formulation of the problem, i.e., the definition of the structure and fluid models, is introduced in Section 2. The discretization of the coupled system is briefly discussed in Section 3. The linear stability problem is posed in Section 4 and the numerical results are discussed in Section 5. The main conclusions are summarized in Section 6.

2. MATHEMATICAL FORMULATION

The rigid cylinder is spring-mounted, damped and immersed in a uniform incompressible viscous flow of velocity $U_\infty \mathbf{i}$ and is free to move in the direction $\mathbf{j}$ orthogonal to the

undisturbed flow. We assume the flow to be two-dimensional and the fluid to be initially at rest. We use a polar reference system (r, θ) centred in the cylinder centre. The lengths are made dimensionless on the cylinder radius R, the velocities using the undisturbed flow velocity U_∞, and the time using the convective scale R/U_∞.

2.1. STRUCTURE MODEL

The law of motion of the rigid cylinder, mounted on a spring and subject to viscous damping and to the fluid action is

$$\frac{d^2 y_c}{dt^2} + \gamma \frac{dy_c}{dt} + \omega_c^2 y_c = \frac{1}{2} n\, c_L(t), \tag{1}$$

where y_c is the position of the centre of the cylinder with respect to its equilibrium solution in the absence of fluid, ω_c is the dimensionless structural natural circular frequency, γ the dimensionless structural damping [equal to twice the structural damping factor multiplied by the structural natural frequency ω_c; see for instance Blevins (1991)], n the fluid/solid density ratio, and c_L the lift coefficient of the cylinder per unit length. The lift coefficient may be obtained [see, for instance, Patel (1978)] as a function of the vorticity distribution ζ on the body surface ($r = 1$ in dimensionless polar coordinated) and its normal gradient $\partial\zeta/\partial r$ at the wall:

$$c_L = \frac{4}{\text{Re}} \int_0^{2\pi} \left(\zeta - \frac{\partial\zeta}{\partial r} \right)_{r=1} \cos\theta\, d\theta, \tag{2}$$

where the ζ term comes from the shear stress contribution and the $\partial\zeta/\partial r$ from the pressure contribution.

2.2. FLUID MODEL

The fluid motion is governed by the continuity equation and the vorticity-transport equation, which is fully equivalent to the Navier–Stokes equations,

$$\frac{\partial\zeta}{\partial t} + \mathbf{v}\cdot\nabla\zeta = \frac{2}{\text{Re}}\nabla^2\zeta. \tag{3}$$

In cylindrical coordinates, the vorticity transport equation reads

$$\frac{\partial\zeta}{\partial t} + v^\theta \frac{1}{r}\frac{\partial\zeta}{\partial\theta} + v^r \frac{\partial\zeta}{\partial r} = \frac{2}{\text{Re}}\nabla^2\zeta. \tag{4}$$

The boundary conditions, enforced on the velocity at the cylinder boundary ($r = 1$ in dimensionless coordinates), are

$$\mathbf{v}(1, \theta) = \mathbf{v}_B, \tag{5}$$

where $\mathbf{v}$ and $\mathbf{v}_B$ denote the velocity of the fluid and of the body boundary. We write the equations in a frame of reference rigidly connected with the structure. In this frame the body velocity $\mathbf{v}_B$ is always zero, but the fluid velocity at infinity is seen as $\mathbf{v}_\infty = \mathbf{i} - v_c\,\mathbf{j}$, with $v_c = \dot{y}_c$ (in dimensionless variables $U_\infty = 1$). The vorticity ζ does not change from one frame to another, as the structure does not rotate but simply translates.

For two-dimensional flows, the formulation used here is a modification of the vorticity–stream function method, in which the ψ–ζ relationship

$$\nabla^2\psi = -\zeta \tag{6}$$

is inverted to yield an integral representation of the velocity in terms of the vorticity. In contrast to Wu (1976, 1982), in order to invert equation (6) and obtain the desired integral form of the ψ–ζ relationship, we use an infinite-space formulation and extend equation (6) to the solid region, with ζ obtained from the prescribed motion of the solid body (assumed to be incompressible). Thus, inverting equation (6) extended to the whole $\mathbb{R}^2$, we have

$$\psi(\mathbf{x}) = \psi_\infty - \iint_{\mathbb{R}^2} G(\mathbf{x}, \mathbf{y}) \zeta(\mathbf{y}) \, dS(\mathbf{y}), \tag{7}$$

where $G(\mathbf{x}, \mathbf{y}) = (1/2\pi) \ln \|\mathbf{x} - \mathbf{y}\|$ is the fundamental solution of the two-dimensional Laplace operator. Equation (7) states that if we know the vorticity in the whole space $\mathbb{R}^2$ (i.e., in the fluid as well in the solid region), then we also know ψ (and hence the velocity) in the whole space $\mathbb{R}^2$. Since the cylinder is in pure translation (without rotation) with respect to the undisturbed flow, $\zeta = 0$ in the solid region. From the definition of the stream function and equation (7) one obtains an integral representation of the velocity field $\mathbf{v}$ in the flow as a function of the vorticity field:

$$\mathbf{v}(\mathbf{x}) = \mathbf{v}_\infty + \mathbf{k} \times \iint_{\mathbb{R}^2} \nabla G(\mathbf{x}, \mathbf{y}) \, \zeta(\mathbf{y}) \, dS(\mathbf{y}), \tag{8}$$

where ∇ denotes the gradient with respect to the variable $\mathbf{x}$, and $\mathbf{k} = \mathbf{i} \times \mathbf{j}$ is the unit vector in the direction normal to the (x, y) plane. In polar coordinates, in a cylinder-based reference frame, equation (8) yields

$$v^\theta = \mathbf{e}_\theta \cdot \mathbf{k} \times \iint_{\mathbb{R}^2} \nabla G \, \zeta \, dS - \sin \theta - v_c \cos \theta,$$

$$v^r = \mathbf{e}_r \cdot \mathbf{k} \times \iint_{\mathbb{R}^2} \nabla G \, \zeta \, dS + \cos \theta - v_c \sin \theta. \tag{9}$$

Within the context of the integral formulation used here, the boundary condition on the cylinder surface, equation (5), needs be imposed only along one direction, because only the ζ scalar field has to be determined on the cylinder boundary. It should be noted that for two-dimensional flows, one may use either the normal or the tangential boundary condition (Wu, 1976, 1982), whereas for three-dimensional flows the normal boundary condition appears more suitable [for a detailed discussion the reader is referred to Morino (1986)]. Let us assume, in particular, the direction of the normal to the wall $\mathbf{e}_r$, which yields

$$\mathbf{e}_r \cdot \mathbf{k} \times \iint_{\mathbb{R}^2} \nabla G \, \zeta \, dS = -\cos \theta + v_c \sin \theta. \tag{10}$$

Enforcing this condition yields a zero-thickness layer of vorticity which immediately diffuses, thereby ensuring that the tangential boundary conditions are satisfied (Lighthill 1963, Batchelor 1967). All the results presented here are obtained using a projection technique, related to the work of Wang & Wu (1986), which yields the same algorithm for both the tangential and the normal approach. Finally, as shown by Wu (1976), in the case of external two-dimensional flows on a body of finite extension, the conservation of total vorticity must be enforced to obtain a unique solution when equation (10) is "inverted" in order to determine the vorticity distribution on the cylinder boundary. This condition is obtained by noting that, according to Kelvin's theorem, $d\Gamma_\infty/dt = 0$, where

$$\Gamma_\infty(t) = \int_{\mathbb{C}_\infty} \mathbf{v} \cdot d\mathbf{x} = \iint_{\mathbb{R}^2} \zeta(\mathbf{y}, t) \, dS(\mathbf{y}). \tag{11}$$

Recalling that we have assumed the fluid to be initially at rest, we have $\Gamma_\infty(0) = 0$ and hence $\Gamma_\infty(t) = 0$ for all t.

3. DISCRETIZED EQUATIONS AND BOUNDARY CONDITIONS

The above integro-differential formulation is discretized in space in order to obtain a set of ordinary differential equations that will be studied by a classical dynamical-system approach. The computational domain extends from the cylinder surface to r_{max} typically of order of 50 cylinder radii. This domain is discretized in polar coordinates with a uniformly spaced grid in the azimuthal coordinate θ and an exponential stretch in the radial coordinate r. The nodes where the vorticity is always negligible are not considered in the computation. The state vector $\mathbf{s}$ of the discrete system is composed of the vorticity values in the nodes in the vortical region (in the fluid), of the total vorticity Γ_E outside the computational domain and of the circular cylinder position y_c and velocity v_c.

We can eliminate from the discretized vorticity-transport equation the velocity [using the discretized form of equation (8)] and the vorticity at the body-boundary nodes [using the discretized form of equation (10)], so as to obtain a vorticity-only formulation. As pointed out above, enforcing the boundary condition yields a zero-thickness vortex layer which then diffuses into a finite-thickness one. In the discretized formulation, we combine the two processes and assume that a finite-thickness layer of vorticity is generated at once. This is accomplished automatically by expressing the vorticity field as

$$\zeta(\mathbf{x}, t) = \sum_{n=1}^{N_T} \zeta_n(t) f_n(\mathbf{x}), \tag{12}$$

where $f_n(\mathbf{x})$ denotes a suitable finite-element-like basis and $\zeta_n(t)$ denotes the value of the vorticity at the node n (imposing the boundary condition determines the layer of vorticity connected with the values of ζ_n at the boundary nodes). The issue of the boundary condition discretization is treated in some detail in Cossu (1997) and Cossu & Morino (1997). Once the vorticity values at the nodes on the cylinder surface are expressed as a function of the state variables (i.e., of the vorticity in the field, the external total vorticity and the structure position and velocity), we can proceed to discretize the vorticity transport equation.

The differential terms appearing in equation (4) are discretized using classical finite difference formulae fourth-order accurate except near the boundaries where they are second-order accurate. We thus obtain, for the nodes $\mathbf{x}_i$ inside the fluid

$$\{\nabla^2 \zeta(\mathbf{x}_i)\} = \mathbf{M}^D \mathbf{s} + \mathbf{e}^D,$$

$$\{\partial \zeta / \partial r(\mathbf{x}_i)\} = \mathbf{M}^R \mathbf{s} + \mathbf{e}^R,$$

$$\{(1/r)\, \partial \zeta / \partial \theta(\mathbf{x}_i)\} = \mathbf{M}^T \mathbf{s} + \mathbf{e}^T. \tag{13}$$

The velocity field can be evaluated at each node by discretizing the integrals in equation (9), the integrals being evaluated using BEM-like techniques, so as to obtain

$$\{v^r(\mathbf{x}_i)\} = \mathbf{M}^{UR} \mathbf{s} + \mathbf{e}^{UR},$$

$$\{v^\theta(\mathbf{x}_i)\} = \mathbf{M}^{UT} \mathbf{s} + \mathbf{e}^{UT}. \tag{14}$$

Finally, combining the discretized differential operators (13) [see Cossu (1997), or Cossu & Morino (1997) for details], the discretized integral representation of the vorticity field (14), the discretized version of the equation of vorticity conservation (11) and the equation of

structural motion equation (1), with a discretized evaluation of the lift coefficient, as given by equation (2), one obtains the space-discretized system of equations for the state vector $\mathbf{x}$

$$\dot{\mathbf{s}} = \mathbf{c} + \mathbf{As} + \mathbf{b}(\mathbf{s}, \mathbf{s}). \tag{15}$$

4. GLOBAL STABILITY ANALYSIS

We denote by $\mathbf{s}_S$ the steady-state solution of equation (15), which satisfies the equation

$$\mathbf{c} + \mathbf{As}_S + \mathbf{b}(\mathbf{s}_S, \mathbf{s}_S) = \mathbf{0}, \tag{16}$$

and is calculated by a sequential Newton–Raphson algorithm marching in the Reynolds number. By symmetry considerations it is easily seen that this solution corresponds to a zero displacement and zero velocity of the cylinder and to a velocity field symmetric with respect to the axis centred in the cylinder centre and parallel to the undisturbed flow. The vorticity field associated with the steady-state solution $\mathbf{s}_S$ is the same as in the case of a stationary cylinder so that $\mathbf{s}_S$ is a function of the Reynolds number but not of the other parameters (ω_c, γ and n). Setting $\mathbf{s} = \mathbf{s}_S + \mathbf{s}_P$ and recalling that $\mathbf{s}_S$ satisfies equation (16), one obtains

$$\dot{\mathbf{s}}_P = \mathbf{A}_P \mathbf{s}_P + \mathbf{b}(\mathbf{s}_P, \mathbf{s}_P), \tag{17}$$

with $\mathbf{A}_P \mathbf{s}_P := \mathbf{As}_P + \mathbf{b}(\mathbf{s}_S, \mathbf{s}_P) + \mathbf{b}(\mathbf{s}_P, \mathbf{s}_S)$. The matrix $\mathbf{A}_P$ is the linearized discretized Navier–Stokes operator that is recovered when terms of order higher than the first in the perturbation vector $\mathbf{s}_P$ are neglected. The eigenvalues of $\mathbf{A}_P$ determine the linear (global) stability of the system and its eigenvectors are the global modes. $\mathbf{A}_P$, and thus its eigenvalues and eigenvectors, depend upon all the parameters of the problem (Re, ω_c, γ, n). The full spectrum of the "purely fluid" (stationary structure) system has been studied in some detail (Cossu 1997) and confirms the well-known result that two complex conjugate eigenvalues cross the imaginary axis at a Reynolds number of about 47 with an imaginary part of about $\omega_0 = 0.37$ corresponding to a Strouhal number St $= \omega_0/\pi = 0.117$. When the cylinder is free to move in the transverse direction, the system has two more degrees of freedom (the cylinder position y_c and velocity v_c) and displays two additional eigenvalues with respect to the stationary-structure case. In the absence of fluid, the system admits only the two structural eigenvalues given by

$$\lambda_s = -\frac{\gamma}{2} \pm i \sqrt{\omega_c^2 - \left(\frac{\gamma}{2}\right)^2}. \tag{18}$$

In the presence of fluid, but for $n \ll 1$, two "nearly-structural" eigenvalues with $\lambda \sim \lambda_s$ are expected. The corresponding eigenvectors are structure-driven vorticity fields in the wake. As soon as one increases the fluid/solid density ratio n, the aerodynamic feedback on the structure becomes more important and the whole spectrum is changed by this interaction. Some interesting questions arise, as follows.

(a) Can the nearly-structural mode become critical as the density ratio n is increased?
(b) Does the critical Reynolds number increase or decrease by increasing the density ratio n?
(c) How does the shape of the nearly-structural mode change if we change the frequency ratio $\Omega_0 = \omega_c/\omega_0$ at a given Reynolds number?
(d) Is chaotic behaviour possible for the coupled system near the bifurcation threshold?

In the following, we try to partially answer these questions by numerically computing the eigenvalues and eigenvectors of the discrete linearized operator $\mathbf{A}_P$ for some suitable set of

parameters. The number of parameters sets considered is limited because each test requires significant computational resources; however, we think that some insight into the problem can be given from the results discussed below.

5. NUMERICAL RESULTS

The computational domain extends from the cylinder surface to 50 cylinder radii in the radial direction and has been discretized with 96 intervals in the azimuthal coordinate and with 48 intervals in the radial direction. As stated above, the grid nodes where the vorticity is always negligible are not considered in the computation and thus the results were obtained with 2762 nodes instead of 4512. The grid is shown in Figure 1. When the structure is stationary, a critical Reynolds number of 47·0244 and a critical frequency of 0·369 (corresponding to a critical Strouhal number equal to 0·1174) are found. The eigenvalues and eigenvectors of $\mathbf{A}_P$ are numerically computed, with a QR algorithm, using the LAPACK routines (Anderson *et al.* 1992). The rightmost part of the spectrum at the Hopf bifurcation for the stationary-structure case is shown in Figure 2: the critical von Karman eigenvalues are on the imaginary axis; the associated vorticity fields are shown in Figure 3. The von Karman mode shape has been extensively analysed (Jackson 1987; Noack & Eckelmann 1994; Cossu 1997) and the reader is referred to these works for further details.

5.1. INFLUENCE OF THE FREQUENCY RATIO

We consider how the frequency ratio Ω_0 affects the spectrum of the coupled system. The parameter Ω_0 is the ratio of the natural circular frequency ω_c of the undamped ($\gamma = 0$) structural oscillator in the absence of fluid to the circular frequency ω_0 of the undamped purely fluid "oscillator", i.e., the frequency of the critical mode at the Hopf bifurcation when the structure is not allowed to move. We analysed the effect of Ω_0 on the spectrum for a low density ratio $n = 1/7000$ (approximatively steel in air) and a small structural damping, $\gamma = 0.01$, so as to avoid the coalescence of the nearly-structural eigenvalues with the von Karman eigenvalues. The Reynolds number was kept fixed at its critical value in the stationary-structure case ($Re_c = 47.024$), where the critical eigenvalues were $\pm i\omega_0 = \pm 0.368865$ i. In Table 1, we report the numerical results for the two least stable pairs of eigenvalues $\lambda_{1,2}$ and $\lambda_{3,4}$. In the same table the "structural" λ_s eigenvalues, given by equation (18), that would have been observed in the absence of fluid, are also reported. Three frequency ratios were considered: the unitary ratio, the ratio $\Omega_0 = 1.8$ [used by Schumm *et al.* (1994), to control the von Karman instability by forced transverse oscillation] and its inverse $\Omega_0 = 0.55$. Both the nearly-structural and the von Karman eigenvalues are insensitive to the aeroelastic coupling and, for the set of parameters considered, the von Karman mode is always the critical one.

When $\Omega_0 = 1$, the shape of the nearly-structural mode almost coincides with the von Karman one (shown in Figure 3) except for a phase shift. This is confirmed by the analysis of Figure 4 where their vorticity normalized values (the shift has been set equal to zero in order to compare the two modes) on the downstream symmetry axis are shown. If we were able to "suppress" the von Karman mode and let the cylinder free to oscillate in the transverse direction at the stationary-cylinder critical Reynolds number and the corresponding characteristic Strouhal frequency, we would observe, for small oscillations, the same disturbance vorticity field in the wake as that for a stationary-cylinder. It would be interesting to study the nonlinear behaviour of the system for $\Omega_0 = 1$ because two nearly identical complex modes interact nonlinearly with nearly identical characteristic frequencies, so that very strong resonances are expected.
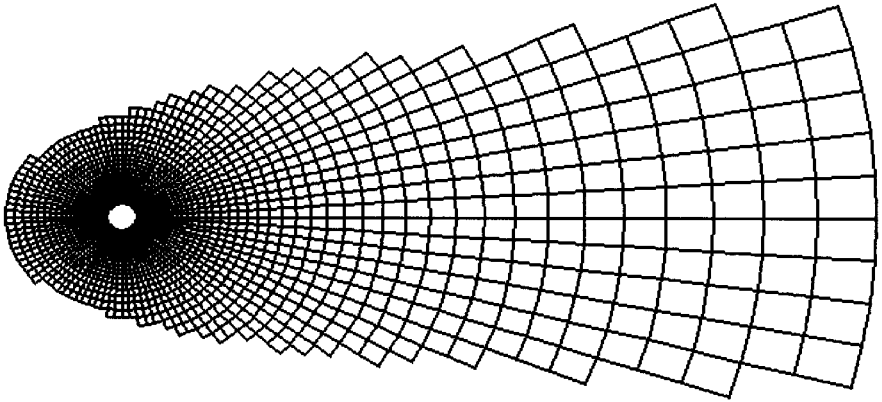
Figure 1. Grid used to discretize the Navier-Stokes equations. The grid nodes where the vorticity is negligible are not included in the computational domain.
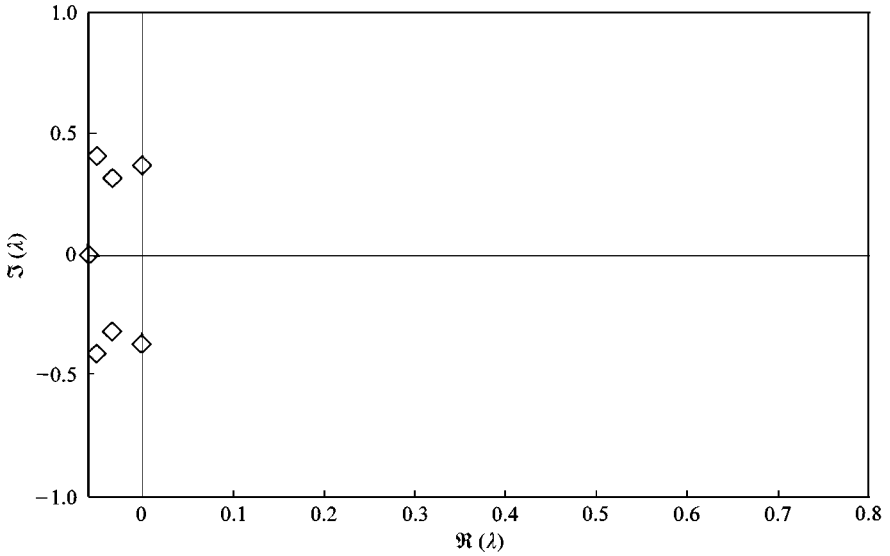
Figure 2. Rightmost part of the spectrum of the linearized Navier–Stokes operator at the Hopf bifurcation (Re = 47·024), for the stationary structure.

TABLE 1

Effect of the frequency ratio Ω_0 on the four leading eigenvalues $\lambda_{1,2}$, $\lambda_{3,4}$ of the coupled system for Re = 47·024, $\gamma = 0·01$ and $n = 1/7000$. The purely structural eigenvalues, given by equation (18), are also reported for comparison. The stationary-structure von Karman eigenvalues, at the same Reynolds number, are $\pm 0·368865$ i

Ω_0	$\lambda_{1,2}$	$\lambda_{3,4}$	λ_s
0·55	$-5·398\ 10^{-5} \pm 0·368$ i	$-4·077\ 10^{-3} \pm 0·204$ i	$-5·0\ 10^{-3} \pm 0·204$ i
1·00	$3·640\ 10^{-4} \pm 0·367$ i	$-4·597\ 10^{-3} \pm 0·369$ i	$-5·0\ 10^{-3} \pm 0·368$ i
1·80	$1·732\ 10^{-5} \pm 0·368$ i	$-4·555\ 10^{-3} \pm 0·663$ i	$-5·0\ 10^{-3} \pm 0·663$ i
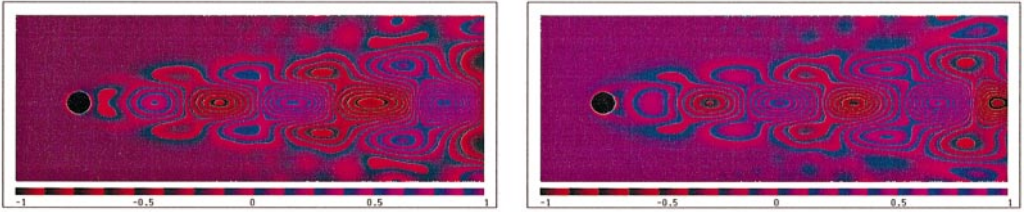
Figure 3. Real and imaginary parts of the von Karman mode at the Hopf bifurcation (Re = 47·024) for the stationary structure.
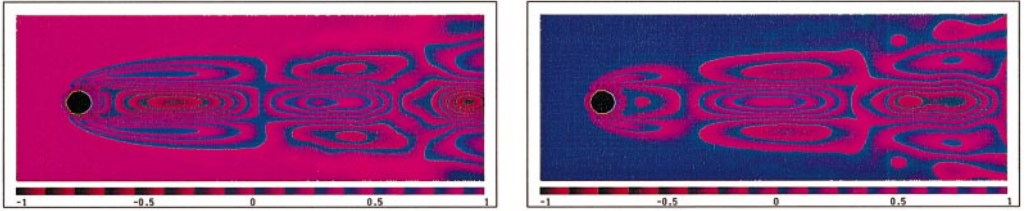
Figure 5. Real and imaginary parts of the disturbance vorticity field associated with the nearly-structural mode for $\Omega_0 = 0.55$, $\gamma = 0.01$, $n = 1/7000$ and Re = 47·024.
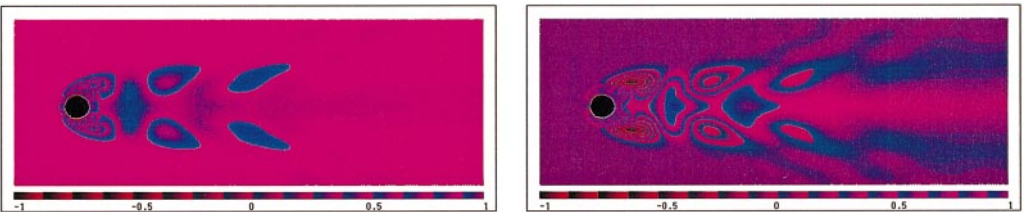
Figure 6. Real and imaginary parts of the disturbance vorticity field associated with the nearly-structural mode for $\Omega_0 = 1.8$, $\gamma = 0.01$, $n = 1/7000$ and Re = 47·024.
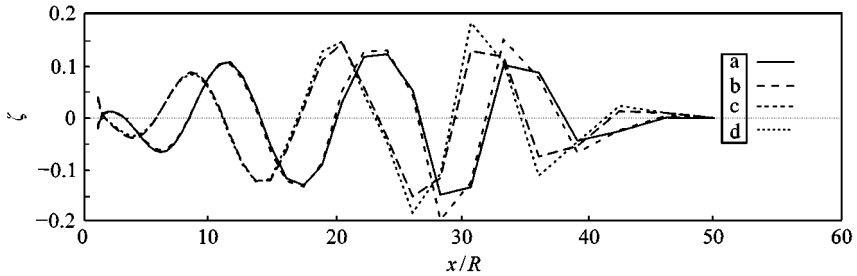
Figure 4. Shape of the vorticity modes on the symmetry axis with density ratio $n = 1/7000$ and frequency ratio $\Omega_0 = 1$: (a) real part of von Karman mode; (b) imaginary part of von Karman mode; (c) real part of the structural mode; (d) imaginary part of the structural mode.

In Figure 5 and 6 the vorticity fields associated with the real and imaginary parts of the "nearly-structural" modes are shown for the values $\Omega_0 = 0.55$ and 1.8. Since the Reynolds number is constant, the mean advection velocity does not change; therefore, if the oscillation frequency is increased, it can be argued that the streamwise wavenumbers will also increase. This is confirmed by the analysis of the modes shown in Figures 5 and 6. In the numerical simulation one has to be careful of this wavenumber change. For too large Ω_0, the wavelength can become too small for the resolution of the chosen grid. For low Ω_0, the wavelength can be too large compared to the numerical solution domain. In Figures 3, 5 and 6 it can also be observed that, as the structural frequency is increased, the disturbance vorticity has a tendency to concentrate upstream. This mode deformation is similar to the one observed as the Reynolds number is increased in stationary bluff-body wakes (Goujon-Durand *et al.* 1994); indeed, in the post-critical behaviour following the first Hopf bifurcation, the Strouhal frequency of the stationary cylinder wake increases with the Reynolds number (Williamson 1996). Therefore, one can conjecture that the von Karman mode deformation, observed when the Reynolds number is increased, in the classical stationary-structure case, is basically due to the increasing intrinsic frequency of the oscillator: at a given Reynolds number the deformed mode is thought to be similar to the one induced by forced transverse oscillation at a frequency corresponding to the characteristic Strouhal number at that Reynolds number.

5.2. INFLUENCE OF THE DENSITY RATIO

The results discussed in Section 5.1 were obtained with a very small density ratio ($n = 1/7000$) and in this case the structure and the fluid were almost uncoupled, i.e., the spectrum of the coupled system was almost the "sum" of the spectra of the "purely fluid" (stationary-structure) system and the "purely structural" (no fluid) one. We now concentrate on the effects of a change in the density ratio n. When n is increased, the aerodynamic forces become of the same order of magnitude of the structural ones, and some changes are expected in the spectrum.

We considered a frequency ratio $\Omega_0 = 1.8$ and a structural damping $\gamma = 0.01$. For these parameters the "purely structural" eigenvalues, given by equation (18), are $\lambda_s = -0.5 \times 10^{-3} \pm 0.663\,i$. Four sets of parameters were considered and the results are reported in Table 2. In the first two tests (first two rows in the table), the Reynolds number was kept at the stationary-structure critical value (Re $= 47.0244$). In this case, an increase of the density ratio n from $1/7000$ to $1/700$ did not substantially affect the spectrum as seen from Figure 7, where the spectra of these two cases are reported. From the first two rows of Table 2, it is
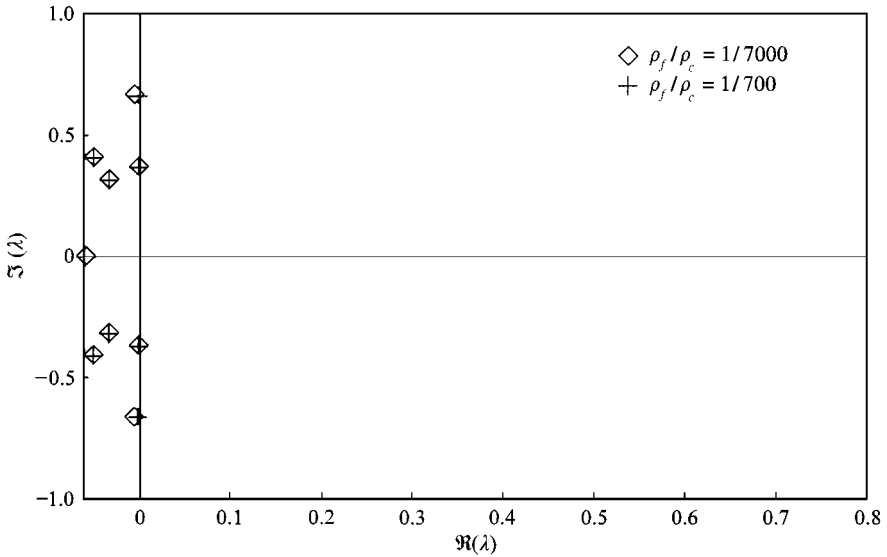
Figure 7. Rightmost part of the spectra of the coupled aeroelastic system corresponding to the first two rows of Table 2: two density ratios $n = 1/7000$ and $1/700$ are considered for $Re = 47 \cdot 024$, $\Omega_0 = 1 \cdot 8$ and $\gamma = 0 \cdot 01$.

TABLE 2

Effect of the density ratio n on the four leading eigenvalues $\lambda_{1,2}$, $\lambda_{3,4}$ of the coupled system for $\Omega_0 = 1 \cdot 8$ and $\gamma = 0 \cdot 01$. In the two upper rows the Reynolds number is chosen at its critical value in the stationary-cylinder case while in the third and fourth rows it is taken equal to half that value. The purely structural eigenvalues λ_s, given by equation (18), are also reported for comparison

n	Re	$\lambda_{1,2}$	$\lambda_{3,4}$	λ_s
1/7000	47·024	$1 \cdot 732 \ 10^{-5} \pm 0 \cdot 368 \ i$	$-4 \cdot 555 \ 10^{-3} \pm 0 \cdot 663 \ i$	$-5 \cdot 0 \ 10^{-3} \pm 0 \cdot 663 \ i$
1/700	47·024	$1 \cdot 705 \ 10^{-4} \pm 0 \cdot 368 \ i$	$-5 \cdot 277 \ 10^{-4} \pm 0 \cdot 663 \ i$	$-5 \cdot 0 \ 10^{-3} \pm 0 \cdot 663 \ i$
1/70	23·512	$3 \cdot 803 \ 10^{-2} \pm 0 \cdot 660 \ i$	$-4 \cdot 385 \ 10^{-2} \pm 0 \cdot 302 \ i$	$-5 \cdot 0 \ 10^{-3} \pm 0 \cdot 663 \ i$
1/7	23·512	$6 \cdot 855 \ 10^{-1} \pm 0 \cdot 097 \ i$	$-4 \cdot 360 \ 10^{-2} \pm 0 \cdot 304 \ i$	$-5 \cdot 0 \ 10^{-3} \pm 0 \cdot 663 \ i$

also seen that the von Karman eigenvalues remain the leading ones ($\lambda_{1,2}$). The nearly-structural eigenvalues $\lambda_{3,4}$ slightly shift to the right in the complex plane as n is increased from 1/7000 to 1/700. Even if they are not strictly unstable they are almost critical and well separated from the remaining stable part of the spectrum so that the corresponding complex mode can also can be considered "active". In that case the system admits four real degrees of freedom and chaotic behaviour is possible near the global bifurcation.

In the next two tests (third and fourth rows in Table 2) the Reynolds number was kept fixed at half the critical stationary-structure value, i.e., $Re = 23 \cdot 512$. Two density ratios were considered: $n = 1/70$ and $1/7$, which approximatively corresponds to steel in water. As seen from Figure 8, where the spectra of these two cases are reported, for these sets of parameters the von Karman mode is stable, while the former nearly-structural one is unstable. The stable part of the spectrum does not seem to be affected by the change in n. The critical Reynolds number, for $n > 1/70$, is less than half the one for the stationary-structure case; however, in that range only a (complex) mode is unstable and chaotic behaviour seems not
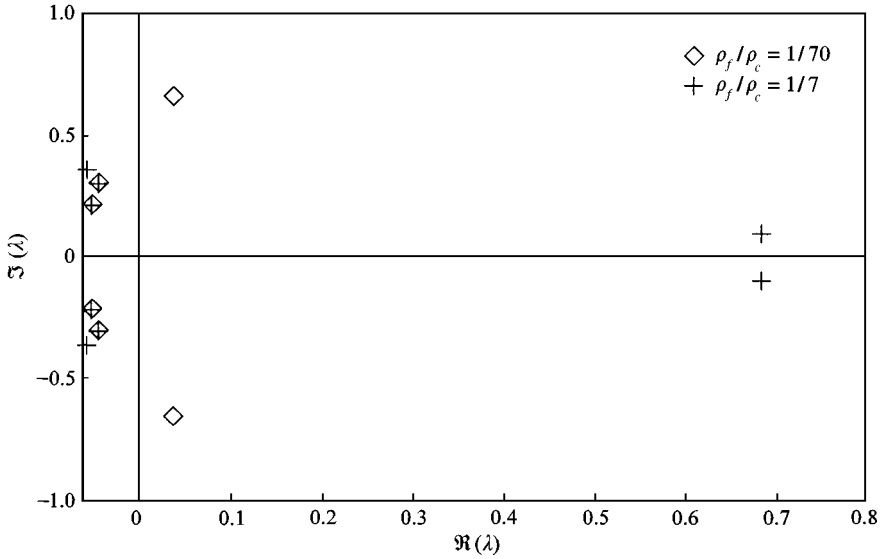
Figure 8. Rightmost part of the spectra of the coupled aeroelastic system corresponding to the third and fourth rows in Table 2: two density ratios $n = 1/70$ and $1/7$ are considered for Re $= 23\cdot512$, $\Omega_0 = 1\cdot8$ and $\gamma = 0\cdot01$.

possible near the bifurcation threshold. For $n = 1/70$ this mode seems to be a nearly-structural one because it has almost the same imaginary part. A further increase in n, from $1/70$ to $1/7$, leads to a strong increase of the growth rate of the unstable mode and to a decrease of its oscillation frequency.

6. CONCLUSIONS

The first instability of a spring-mounted, damped rigid circular cylinder in a viscous flow has been numerically investigated without resorting to any semi-empirical modelling. An integro-differential vorticity-only formulation has been adopted for the full Navier–Stokes equations, used to model the flow around the moving structure.

Two significant modes are identified: the "nearly-structural" one and the von Karman one. The nearly-structural mode corresponds to eigenvalues which, in the limit of very small fluid/solid density ratios n, tend to the characteristic (complex) frequency of the structure in the absence of fluid. The von Karman mode corresponds to a pair of eigenvalues whose frequencies are almost identical to the leading eigenvalues of the "purely fluid" system with a stationary-structure near bifurcation. These two modes are well defined only for low ratios of the fluid density to the structure density.

We first analysed the effect of a change in the frequency ratio Ω_0, for a low density ratio and a Reynolds number equal to the stationary-structure critical value. Both the nearly-structural and the von Karman eigenvalues have been seen to be quite insensitive to the aeroelastic coupling at the considered very small $n = 1/7000$, i.e., for steel in air. When $\Omega_0 = 1$ the nearly-structural complex mode almost coincides with the von Karman one except for a phase shift. An increase of Ω_0, with a constant Re, produces a deformation of the nearly-structural mode which is similar to the one observed when the Reynolds number is increased in the stationary-structure case.

The effect of a change in density ratio n was also considered for a fixed Ω_0. An increase of the density ratio n from $1/7000$ to $1/700$ did not substantially affect the spectrum. The von

Karman mode remained the critical one, while the nearly-structural mode is almost critical but not strictly unstable. For higher n the situation greatly changes. The critical Reynolds number for $n = 1/70$ is less than the half that of the stationary-structure case. A further increase in n leads to a strong increase of the growth rate of the unstable mode and to a decrease of its frequency. For $n > 1/70$, for the sets of parameters considered, just a complex mode is unstable and no chaotic behaviour seems possible near the bifurcation, while for $n < 1/700$ and low structural damping two complex modes are critical; in that case the system admits four active real degrees of freedom and chaotic behaviour is possible near the bifurcation (Guckenheimer & Holmes 1986). In future work, the effect of structural damping and the weakly nonlinear interaction of the von Karman mode and the nearly-structural one will be studied.

ACKNOWLEDGMENTS

REFERENCES

ABARBANEL, S. S., DON, W. S., GOTTLIEB, D., RUDY, D. H. & TOWNSEND, J. C. 1991 Secondary frequencies in the wake of a circular cylinder with vortex shedding. *Journal of Fluid Mechanics* **225,** 557–574.

ANDERSON, E., BAI, Z., BISHOF, C., DEMMEL, J., DONGARRA, J., DU CROZ, J., GREENBAUM, A., HAMMARLING, S., MC KENNEY, A., OSTUCHOV, S., & SORENSEN, D. 1992 *LAPACK Users' Guide*. Philadelphia: SIAM.

VAN ATTA, C. W. & GHARIB, M. 1987 Ordered and chaotic vortex streets behind circular cylinders at low Reynolds number. *Journal of Fluid Mechanics* **174,** 113–133.

BATCHELOR, G. K. 1967 *An Introduction to Fluid Dynamics*. Cambridge, U.K.: Cambridge University Press.

BLEVINS, R. D. 1991 *Flow-Induced Vibrations*. New-York: Van Nostrand Reinhold.

COSSU, C. 1997 Linear and nonlinear stability analysis of a viscous flow around a circular cylinder Ph.D. Thesis in Aerospace Engineering, Università *La Sapienza*, Roma, Italy (in Italian).

COSSU, C. & MORINO, L. 1997 A vorticity-only formulation and a low-order asymptotic expansion near Hopf bifurcation. *Computational Mechanics* **20,** 229–241.

GOUJON-DURAND, S., JENFFER, P. & WESFREID, J. E. 1994 Downstream evolution of the Bénard-von Kármán instability. *Physical Review E* **30,** 308–313.

GUCKENHEIMER, J. & HOLMES, P. 1986 *Nonlinear Oscillations, Dynamical Systems and Bifurcations of Vector Fields*. New York: Springer-Verlag.

HUERRE, P. & MONKEWITZ, P. A. 1990 Local and global instabilities in spatially developing flows. *Annual Review of Fluid Mechanics* **22,** 473–537.

JACKSON, C. P. 1987 A finite-element study of the onset of vortex shedding in flow past variously shaped bodies. *Journal of Fluid Mechanics* **182,** 23–45.

LIGHTHILL, M. J. 1963 Introduction to boundary-layer theory. In *Laminar Boundary Layers* (ed. L. Rosenhead), pp. 46–113. Oxford, U.K.: Oxford University Press.

MATHIS, C., PROVANSAL, M. & BOYER, L. 1984 The Bénard-von Kármán instability: an experimental study near the threshold. *Journal de Physique*, Lettres **45,** 483–491.

MONKEWITZ, P. A. 1988 The absolute and convective nature of instability in two-dimensional wakes at low Reynolds numbers. *Physics of Fluids* **31,** 999–1006.

MORINO, L. 1986 Helmholtz decomposition revisited: vorticity generation and trailing edge condition. Part 1, incompressible flows. *Computational Mechanics* **1,** 65–90.

NOACK, B. R. & ECKELMANN, H. 1994 A global stability analysis of the steady and periodic cylinder wake. *Journal of Fluid Mechanics* **270,** 297–330.

OLINGER, D. J. 1990 Universality in the transition to chaos in open fluid flows. Ph. D. Thesis, Yale University.

OLINGER, D. J. & SREENIVASAN, K. R. 1988 Nonlinear dynamics of the wake of an oscillating cylinder. *Physical Review Letters* **60,** 797–800.

PATEL, V. A. 1978 Kármán vortex street behind a circular cylinder by the series truncation method. *Journal of Computational Physics* **28,** 14–42.

SCHUMM, M., BERGER, E. & MONKEWITZ, P. A. 1994 Self-excited oscillations in the wake of two-dimensional bluff bodies and their control. *Journal of Fluid Mechanics* **271,** 17–53.

SREENIVASAN, K. R. 1985 Transition to turbulence in fluid flows and low-dimensional chaos. In *Frontiers in Fluid Mechanics* (eds S. H. Davis & J. L. Lumley). New York: Springer-Verlag.

SREENIVASAN, K. R., STRYKOWSKI, P. J. & OLINGER, D. J. 1987 Hopf bifurcation, Landau equation and vortex shedding behind circular cylinders. In *Proceedings of the Forum on Unsteady Flow Separation* (ed. K. N. Ghia), Vol. 52, pp. 1–13, New York: ASME.

WANG, C. M. & WU, J. C. 1986 Numerical solutions of Navier–Stokes problems using integral representation with series expansion. *AIAA Journal* **24,** 1305–1312.

WILLIAMSON, C. H. K. 1996 Vortex dynamics in the cylinder wake. *Annual Review of Fluid Mechanics* **28,** 477–539.

WU, J. C. 1976 Numerical boundary conditions for viscous flow problems. *AIAA Journal* **14,** 1042–1049.

WU, J. C. 1982 Problems of general viscous flows. In *Developments in Boundary Element Methods* (eds. R. P. Shaw & P. K. Banerjee). London: Elsevier Applied Science Publishers.

WU, J. C. & THOMSON, J. F. 1973 Numerical solution of time dependent incompressible Navier–Stokes equations using an integro-differential formulation. *Computer and Fluids* **1,** 197–215.

APPENDIX: NOMENCLATURE

$\mathbf{A}$	linear part of the discretized Navier–Stokes operator
$\mathbf{A}_P$	linearized discretized Navier–Stokes operator
$\mathbf{b}$	bilinear part of the discretized Navier–Stokes operator
$\mathbf{c}$	constant part of the discretized Navier–Stokes operator
c_L	lift coefficient, $L/(\rho_f U_\infty^2/2)$
D	cylinder diameter, $2R$
$\mathbf{e}_r$	unit vector in the radial direction
$\mathbf{e}_\theta$	unit vector in the azimuthal direction
G	Green's function for the Laplacian operator
i	imaginary unit, $\sqrt{-1}$
$\mathbf{i}$	unit vector parallel to the undisturbed flow
$\mathbf{j}$	unit vector orthogonal to the undisturbed flow in the plane of the flow
$\mathbf{k}$	unit vector orthogonal to the plane of the flow
n	fluid/solid density ratio, ρ_f/ρ_c
r	radial coordinate
R	cylinder radius
Re	Reynolds number, $U_\infty D/\nu$
St	Strouhal number, ω/π
v_c	vertical velocity of the cylinder, $\dot{y}_c$
v^r	radial velocity component, $\mathbf{e}_r \cdot \mathbf{v}$
v^θ	azimuthal velocity component, $\mathbf{e}_\theta \cdot \mathbf{v}$
U_∞	magnitude of the freestream velocity in the inertial reference frame
$\mathbf{v}$	velocity field in the fluid
$\mathbf{v}_\infty$	velocity field of the undisturbed flow
$\mathbf{v}_B$	velocity of the structure
$\mathbf{s}$	state vector of the discretized system
$\mathbf{s}_P$	perturbation from the steady state of the discretized system
$\mathbf{s}_S$	steady-state solution of the discretized system
y_c	position of the cylinder centre in the inertial reference frame
γ	structural damping
Γ_∞	global circulation

Γ_E circulation over the domain external to the computational domain
ζ vorticity field
θ azimuthal coordinate
λ eigenvalue of the linearized aeroelastic operator
$\lambda_{1,2}$ leading eigenpair
$\lambda_{3,4}$ second leading eigenpair (excepted $\lambda_{1,2}$)
λ_s structural eigenvalue in the absence of fluid
v kinematic viscosity of the fluid
ρ_c density of the cylindrical structure
ρ_f density of the fluid
ψ stream function
ω_c structural natural circular frequency
ω_0 circular frequency of the von Karman mode at the bifurcation with a stationary-structure
Ω_0 frequency ratio, ω_c/ω_0